nature communications

Article

https://doi.org/10.1038/s41467-025-60743-z

Sulfur isotopes from the lunar farside reveal global volatile loss following the giant impact

Received: 22 February 2025

Accepted: 3 June 2025

Published online: 01 July 2025

Check for updates

Yiheng Li[1,2], Zaicong Wang[1] ✉, Wen Zhang[1], Keqing Zong[1], Zhenbing She[1], Qi He[1], Jiaqi Zheng[1], Tianyang Li[1], Fabin Pan[1], Xu Chen[1], Kosta Crnobrnja[1], Long Xiao[1], Zhaochu Hu[1], Xiang Wu[1], Yongsheng Liu[1], Julien Siebert[2] & Frédéric Moynier[2]

The Moon is strongly depleted in volatile elements and exhibits heavier isotopic signatures (e.g., K, Zn) than the Earth. However, the pronounced nearside–farside dichotomy and uneven distribution of volatiles across lunar interior raise the question of whether such heavier isotopic signatures resulted from a global giant impact or local magmatic processes. Here we report high sulfur contents (1800 ± 400 μg/g) and $\delta^{34}S$ values (0.83 ± 0.16‰, 2SE, n = 17) in Chang'e-6 basalt from lunar farside, with similar $\delta^{34}S$ values in two nonmare crustal clasts. These values fall within the range reported for nearside mare basalts and basaltic meteorites of different ages and mantle sources, indicating a broadly homogeneous $\delta^{34}S$ composition across lunar interior that is ~2‰ heavier than the Earth's mantle. This isotopic signature cannot be explained by core formation or late accretion and is best attributed to global volatile loss during the Moon-forming impact. Subsequent magma ocean evolution and mantle overturn drove heterogeneous volatile budget in lunar mantle.

Current models favor that the Moon formed during an impact between a Mars-size planetary body and the proto-Earth, in which the Moon was derived from a mixture of the impactor and the proto-Earth[1]. Key evidences for this include the nearly identical relative abundances of refractory lithophile elements in both the Earth and the Moon, along with similar isotopic anomaly signatures in elements such as O, Ti, Cr and Ca[2–5]. The pronounced volatile depletion with global enrichments in the heavier isotopes (e.g., S, Cl, K, Rb and Zn)[6–10] implies strong evaporation during its formation[11,12].

Although the lunar interior was previously considered to be devoid of volatiles, the discovery of H, F, Cl, and S in volcanic glasses[13] affected this assumption. Subsequent analyses of these glasses and melt inclusions in Apollo mare basalts have revealed that volatile concentrations could be approaching those of terrestrial mid-ocean ridge basalts (MORB), albeit with significant heterogeneity[14–18]. Such heterogeneity may reflect incomplete accretion during the Moon's formation[1] or subsequent evolutionary processes, including mantle overturn[19,20] or regional degassing[21]. Since isotopes of volatile-element could be fractionated under these conditions, it thus remains unclear whether isotopic data from current lunar sample collections—primarily lunar nearside Procellarum KREEP Terrane (PKT) region—could provide a comprehensive representation of the entire Moon. In particular, samples from the PKT region demonstrate substantial elemental anomalies from the Feldspathic Highlands Terrane and the farside South Pole-Aitken Terrane, such as K, Th and other incompatible elements[22]. Barnes et al.[21] proposed that the enrichment in the heavier Cl isotopes in urKREEP required metal–chloride degassing, inferring that at least one large impact event may have exposed the residual Lunar Magma Ocean (LMO) melt at the lunar surface before complete solidification. If such an event occurred, the volatile elements and

[1]State Key Laboratory of Geological Processes and Mineral Resources, Hubei Key Laboratory of Planetary Geology and Deep-Space Exploration, School of Earth Sciences, China University of Geosciences, Wuhan, China. [2]Universite de Paris Cité, Institut de Physique du Globe de Paris, Centre National de la Recherche Scientifique (CNRS), Unité Mixte de Recherche (UMR) 7154, Paris, France. ✉e-mail: zaicongwang@cug.edu.cn

isotopic compositions in all returned samples from the PKT region may have been altered, thereby not necessarily reflecting the Moon's primordial characteristics[23]. Radiogenic isotopes (e.g., μ values reflecting $^{238}U/^{204}Pb$ ratio) also point to very heterogeneous mantle domains for different mare basalts[24].

Sulfur, a moderately volatile element, could be a revealing tracer of these processes. Given high sulfur contents at sulfide saturation (SCSS) for lunar basalts[25], S hardly reaches sulfide saturation until the late stage of the lunar magmatic evolution[25–27]. Therefore, its isotopes in melts would reflect the primary signature, even after complex LMO overturn and mixing of cumulates[28]. Moreover, previous sulfur isotope studies have shown that mare basalts formed through effusive eruptions experienced minimal degassing (less than 10%) compared to lunar volcanic glasses produced by fire-fountain eruptions[8,28,29]. Thus the sulfur isotopic composition of mare basalts should closely reflect their parental magmas and mantle sources[8,29]. Existing nearside samples, such as Apollo, Chang'e-5 (CE-5) and lunar meteorites, exhibit an overall uniform $\delta^{34}S$ value of 0.6 ± 0.3‰[8,28,29], which is ~2‰ heavier than Earth's sulfur isotope composition[30]. It raises the question of whether farside samples would confirm this homogeneity.

The Chang'e-6 (CE-6) mission returned the first soil samples from a farside mare basalt unit within the Apollo basin[31]. The low-Ti basalt erupted at about 2.8 Ga and originated from a lunar mantle source region that is highly depleted in incompatible elements—a characteristic distinctly different from nearside PKT rocks[32–34]. Consequently, the CE-6 samples are critically important for elucidating the distribution of sulfur on the Moon and assessing the homogeneity of lunar sulfur isotopes. Additionally, the CE-6 soil sample contains rock clasts from both the mantle (e.g., basalt) and the crust (e.g., anorthositic norite and anorthosite), providing integrated information on sulfur isotopes in the lunar farside.

In this work, we conducted a detailed petrological investigation of troilites in basalts, nonmare clasts, and breccias from the CE-6 samples, and carried in-situ high-precision sulfur isotope analyses of these troilites[28]. Given that most of the sulfur in lunar basalts is stored in troilite[28], the sulfur isotopes in troilite can be taken to broadly represent or at least be comparable with the bulk-rock sulfur isotopic composition. Our new findings confirm a homogenous sulfur isotope of the whole lunar interior, and from a volatile element perspective, offer further constraints on models for the Moon's formation.

Results and discussion

Petrography

The CE-6 low-Ti basalt clasts exhibit various basaltic textures (porphyritic, vitrophyric, poikilitic and subophitic) and are primarily composed of clinopyroxene, plagioclase, ilmenite with the minor occurrence of cristobalite, troilite, and apatite (Fig. 1a, b). The nonmare lithologies in CE-6 samples are predominantly composed of plagioclase, accompanied by orthopyroxene and minor troilite (Fig. 1c, d), and are classified as noritic anorthosite and norite[35,36]. According to the Mg# of pyroxene and An# of plagioclases, the two nonmare clasts are chemically closed to Mg suite and Ferroan Anorthosite (FAN) (Fig. S1, Table S1). Polymict breccias contain clasts and rock fragments exhibiting diverse characteristics and complex origins. As illustrated in Fig. 1e, f, basalt clasts, mineral fragments, and impact glasses are all incorporated within the breccia, indicating extensive sputtering and gardening on the CE-6 landing sites.

We selected 40 large basalt clasts from several hundred lunar soil clasts and performed quantitative mineralogical analyses using TESCAN Integrated Mineral Analyzer (TIMA). The results indicate that the CE-6 basalts exhibit 0.31 ± 0.07 (2SE) vol% troilite (Table S2, Fig. S2a). Taking into account the varying densities of different mineral phases and the 36.5 wt% sulfur content of troilite (FeS), the sulfur content of CE-6 basalts can be estimated to be 1800 ± 400 μg/g. Using the same method, the sulfur content of NWA 14526 and NWA 12008 are estimated to be 260 ± 130 μg/g and 400 ± 200 μg/g (Table S1). According to Elardo et al.[37], the troilites abundance of NWA 4734 is 0.1 to 0.3 vol % and the S content is thus estimated to be between 600 and 1700 μg/g.

Most sulfide grains are less than 20 μm in size, with only a few larger than 50 μm (Fig. S2c). Although the basalt clasts exhibit various textures, the troilites mainly occur interstitially, typically associated with late-stage crystallizing minerals such as ilmenite, plagioclase, apatite, and clinopyroxene characterized by low Mg# (<10) (Fig. S2b). In non-mare rock clasts (Fig. 1c, d), sulfides occasionally appear within plagioclase grains, with grain sizes generally below 10 μm. We also found large sulfides occurring in the matrix of breccias (Fig. 1e, f).

Composition of CE-6 troilites

In CE-6 clasts, sulfides largely conform to the formula FeS (troilite, Table S2), which is one of the most common accessory minerals in lunar rocks[38]. Troilites in the basalt clasts display 0.02 to 0.11 wt% Co, <0.04 wt% Ni, and <0.05 wt% Cu. The Co, Ni and Cu contents are within the range of troilites in Apollo basalts[38] and the CE-5 basalt[28]. The composition of troilites is comparable among basalt clasts, nonmare clasts and breccias, except Ni content. Troilites in noritic anorthosite and norite clasts exhibit variably Ni contents, which mainly result from the heterogenous distribution of Ni in microscales (Figs. 2c and S4 and Table S3). In breccias, most troilites Ni concentrations fall within the basaltic range, although some samples display anomalously elevated Ni contents (Fig. S3).

Sulfur isotopes of CE-6 troilites

Nineteen analyses of sulfur isotopes compositions are conducted on troilites in thirteen basaltic clasts by laser-ablation MC-ICP-MS with spot diameter of 8 μm[28] (Table S4, See details in Supplementary methods). To further validate our data, we conducted multiple analyses on sufficiently large troilite grains or different grains from the same clast (Figs. 1 and S5). We found that although most sulfur isotope values from different spots lie within the analytical uncertainty, two analyses from a single grain exhibit a larger discrepancy (1.30 ± 0.24‰ and 2.32 ± 0.47‰; Fig. S5c). Notably, in this basaltic clast, troilite is in contact with pyroxene at the clast's edge, while the clast itself is significantly fractured. As this grain may have been affected by potential degassing, it was excluded from the average value calculation. A similar intra-grain isotopic variation has also been observed in sulfides from CE-5 basalts and lunar meteorites[28,39]. The $\delta^{34}S_{V\text{-}CDT}$ value of troilites in basaltic clasts display a mean value of 0.83 ± 0.16‰ (2SE, n = 17). In addition, we found that most clinopyroxenes coexisting with troilite have Mg# values below 10, indicating their crystallization during the late stage of magma evolution (Fig. 2b). Notably, the troilite in contact with the most primitive clinopyroxene exhibits a $\delta^{34}S_{V\text{-}CDT}$ value of 0.77 ± 0.32‰ (Fig. 2b). The $\delta^{34}S_{V\text{-}CDT}$ values of troilites in NWA 14526 and NWA 12008 are 0.84 ± 0.17‰ (2SE, n = 10) and 0.29 ± 0.31‰ (2SE, n = 7), respectively.

Two nonmare fragments record troilite $\delta^{34}S_{V\text{-}CDT}$ values of 1.14 ± 0.60‰ and 0.94 ± 0.62‰, respectively (Fig. 2a). In breccias, troilite exhibits $\delta^{34}S_{V\text{-}CDT}$ values ranging from 0.30 ± 0.40‰ to 2.19 ± 0.48‰ (Fig. 2a). The mean $\delta^{34}S_{V\text{-}CDT}$ value of troilite in breccias, 1.24 ± 0.31‰ (2SE, n = 14), is slightly higher than that of troilite in CE-6 basalts.

Origin and sulfur isotopes of the troilite in CE-6 samples

The $\delta^{34}S$ values of troilite in CE-6 basalt clasts vary from 0.30 ± 0.51‰ to 1.52 ± 0.37‰. The mean value of 0.83 ± 0.16‰ broadly overlaps with those observed in CE-6 nonmare clasts, Apollo basalts, and lunar meteorites (Fig. 2a). In addition, troilite in the CE-6 breccia displays slightly elevated $\delta^{34}S$ values, with an average of 1.24 ± 0.31‰. In the following sections, we assess the potential influence of meteoritic

https://doi.org/10.1038/s41467-025-60743-z

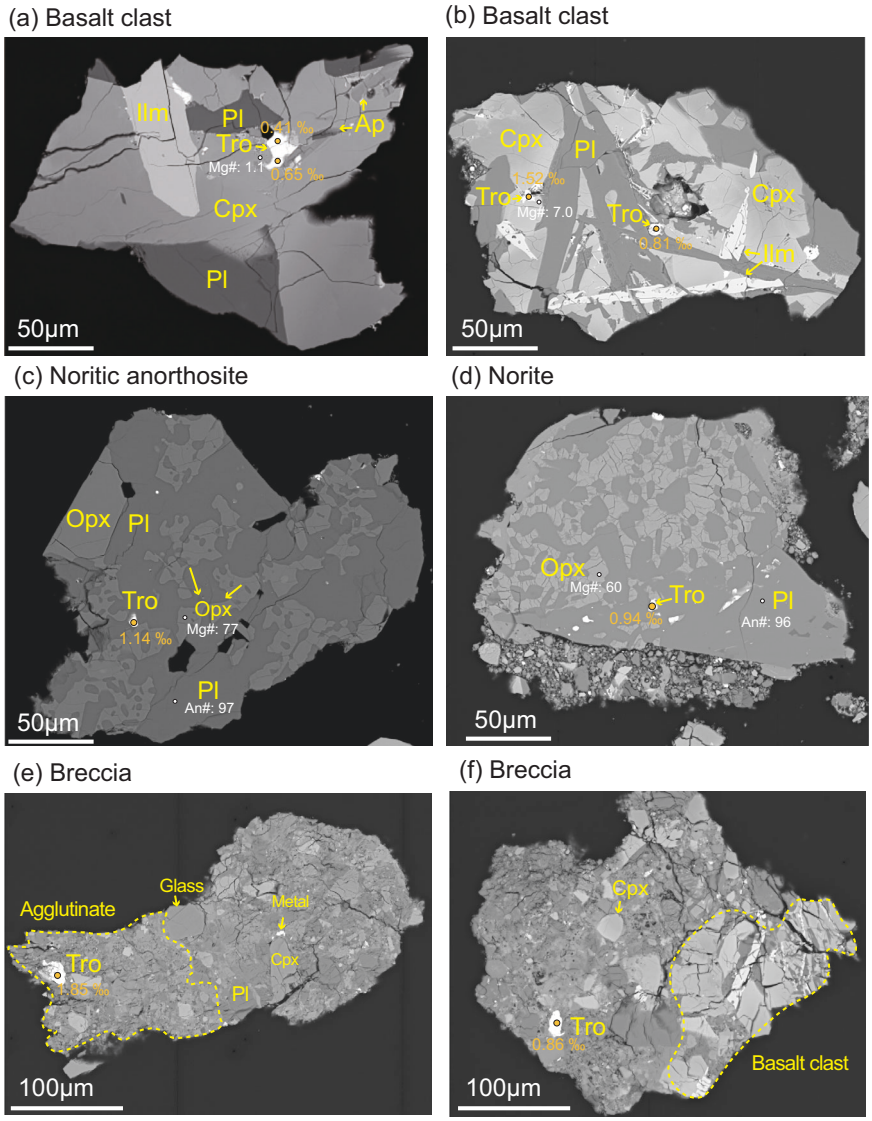

Fig. 1 | Representative lithic clasts in CE-6 soil for sulfur isotope analyses. Large clasts of mare basalts (**a**, **b**), noritic anorthosite (**c**), norite (**d**) and breccia (**e**, **f**) are shown. Orange circles (~8 μm in diameter) mark laser ablation spots for sulfur isotope analyses, with corresponding $\delta^{34}S$ values labeled. The Mg# of clinopyroxene (Cpx) and orthopyroxene (Opx) closely associated with troilites and An# of plagioclase in anorthositic norite are also indicated. Tro troilite, Pl plagioclase, Cpx clinopyroxene, Opx orthopyroxene, Ap apatite, Ilm ilmenite.

impacts, magmatic differentiation, and degassing processes on these isotopic compositions.

The Ni concentration in troilite from CE-6 basalt clasts falls within the range observed for endogenous troilites in Apollo and CE-5 samples (Fig. S4a), consistent with the low bulk Ni content of the CE-6 basalt (~16.2 μg/g[36]). A few troilites in CE-6 breccias exhibit considerable variation in Ni content, reaching 7070–36190 μg/g (Figs. 2c and S4a)—levels akin to those observed in troilite from the CE-5 impact melt[28]. According to current findings, lunar soil and impact glass represent significant reservoirs of heavy sulfur isotopes on the Moon ($\delta^{34}S$ ranging from +4‰ to +58‰), which may be attributed to sulfur evaporation induced by (micro)meteorite impacts or ion sputtering[40–42]. The elevated Ni content and $\delta^{34}S$ values observed in some breccia-hosted troilites could reflect meteorite-induced modification on the CE-6 landing site, though the magnitude of fractionation indicates only limited impact-related alteration on CE-6 breccia.

Early magmatic sulfide segregation could enrich remaining melts in light sulfur isotopes[43]; hence, determining whether CE-6 basaltic magmas reached early sulfide saturation is essential. Most troilites in CE-6 basalts are associated with late-stage minerals and low-Mg clinopyroxenes (Figs. 2b and S2b), suggesting late-stage crystallization. Moreover, a troilite grain coexisting with a primitive clinopyroxene (Mg# 43.9) exhibits $\delta^{34}S$ of 0.77 ± 0.32‰, consistent with late stage-forming troilites (Fig. 2b), indicating limited sulfur isotope variation during magmatic differentiation.

Sulfide saturation is typically evaluated using the SCSS, which is sensitive to temperature, pressure, and melt composition. Experimental studies conducted under lunar conditions suggest that most basaltic magmas have SCSS values (>2600 μg/g)[25,27] that exceed the sulfur contents of mare basalt, implying sulfur-undersaturated evolution. While SCSS can be significantly lowered under highly reduced conditions due to the presence of Fe-rich, S-poor, or Ni-rich sulfides[27,44], troilite in CE-6 basalt clasts exhibits a stoichiometric FeS composition (metal/sulfur = 1.0), and the bulk Ni concentration of CE-6 basalt is low (~16.2 μg/g, Fig. S6), rendering these scenarios unlikely. Using the sulfur solubility model of Ji and Dasgupta[27], and applying pressure-temperature conditions analogous to those of CE-5 basalts (1250–1550 °C, 1–1.5 GPa) due to compositional and mineralogical

https://doi.org/10.1038/s41467-025-60743-z

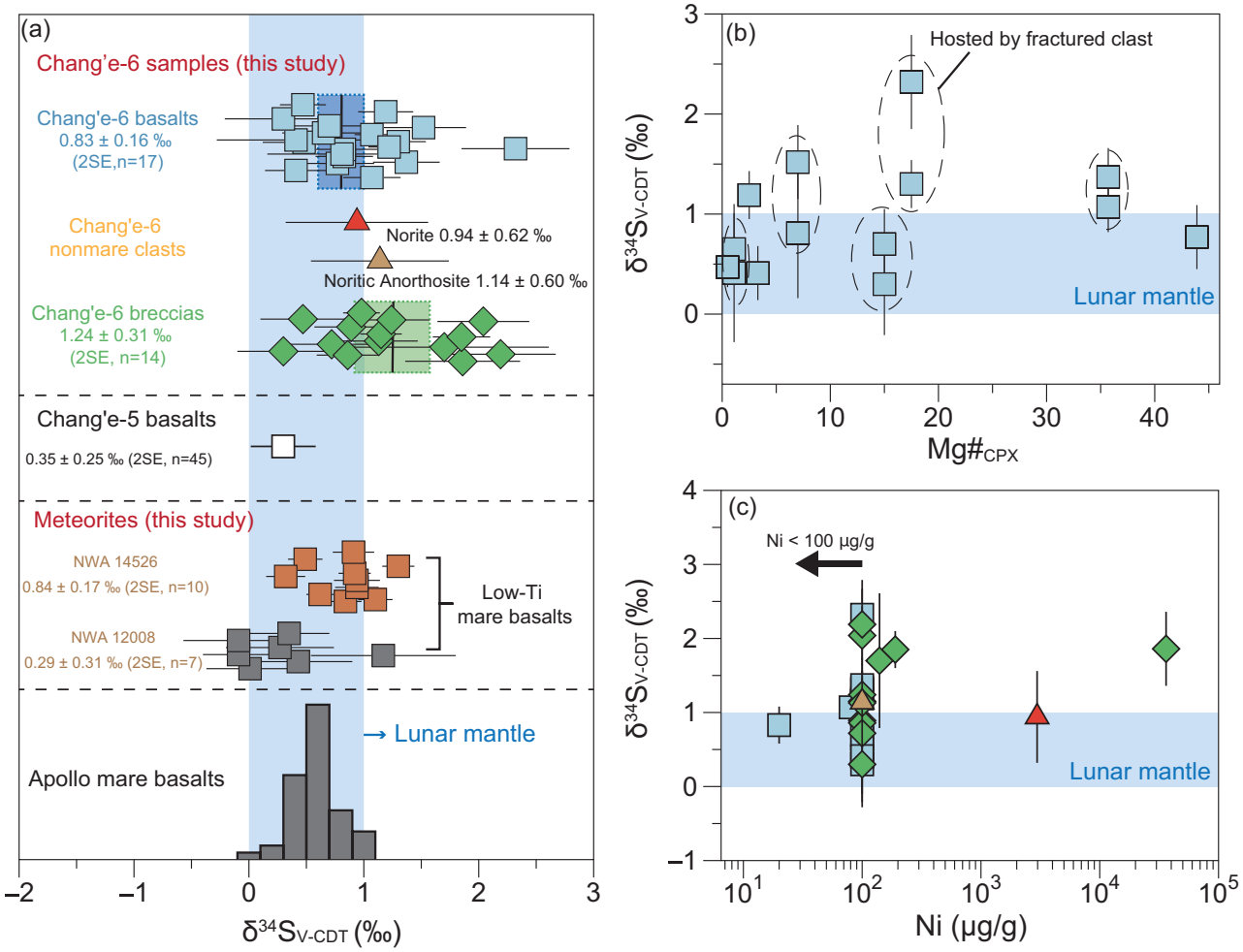

Fig. 2 | Sulfur isotopes ($\delta^{34}S$) of troilites in the basalt clasts, breccias and nonmare clasts in CE-6 soil and lunar meteorites analyzed in this study. Bulk rock $\delta^{34}S$ values of Apollo basalts[8,28,29] and CE-5 basalts[28,39] are shown for comparison (**a**). $\delta^{34}S$ values and Mg# of associated clinopyroxene are plotted in (**b**). Data enclosed by the dashed black circle in (**b**) represent troilites from the same clast or grain. **c** shows Ni content versus $\delta^{34}S$ for the same troilite grain. Error bars represent ±2 standard errors (2SE) of $\delta^{34}S$ measurements.

similarities, we estimate SCSS values for CE-6 magmas in the range of 3420–5760 μg/g. This range far exceeds the measured sulfur content (1800 ± 400 μg/g), suggesting a sulfur-undersaturated evolution at the early stage of magmatism (Fig. 3a). Furthermore, copper, being both incompatible and chalcophile, is sensitive to sulfide segregation. Early sulfide saturation would markedly lower Cu concentrations in the residual melt[45]. The relatively high Cu contents observed in CE-6 and CE-5 basalts (Fig. 3b) further support the absence of early sulfide segregation during magmatic evolution, as well shown in most mare basalts[45]. In fact, the incompatible behavior of S and other chalcophile elements supports the sulfur-undersaturated evolution for the lunar mare basalts[45]. Such a conclusion is also supported by the petrological evidence that most troilites formed at late stages of magmatic evolution (Figs. 1a, b and S5).

The influence of degassing on sulfur isotopes during lunar magmatism is largely governed by the eruption style (fire-fountain eruptions or effusive eruption)[29,46]. According to the model by Saal and Hauri[46], fire-fountain eruptions, such as those that produced volcanic glasses, occur under conditions where the ratio of the effective vapor pressure of sulfur to its saturation pressure (P/P_{Sat}) approaches 1. Degassing under such near-saturation conditions (with a fractionation factor $\alpha_{gas-melt} = 1.003$) could progressively enriched the residual melt in lighter sulfur isotopes ($\delta^{34}S$ value ranging from +1.3‰ to −14.0‰)[46] (Fig. 4a). In contrast, CE-6 basalts are interpreted as typical mare basalts formed by effusive eruptions. Any degassing in these lavas would have occurred near the lunar surface under low P/P_{Sat} conditions (e.g., <0.86)[8,29], where kinetic isotope fractionation dominates—similar to that observed during impact-related sulfur volatilization (Fig. 4a). Notably, even modest sulfur loss (~20%) under vacuum conditions can induce substantial isotopic enrichment in the residual melt (e.g., a + 7‰ $\delta^{34}S$ shift)[8,29] (Fig. 4b). In-situ $\delta^{34}S$ values of troilite in most CE-6 basalt clasts fall within a relatively narrow range (~1.2‰, noting the external uncertainty of ±0.50‰), suggesting that the sulfur loss during magma emplacement was minimal, likely less than 10%[8]. Moreover, olivine-hosted melt inclusions of Apollo mare basalts—typically considered to be unaffected by degassing—exhibit $\delta^{34}S$ values ranging from −0.30 ± 0.91‰ to 1.6 ± 1.81‰[46]. These values closely match those of troilite in our study, further supporting the interpretation that the CE-6 basalts experienced limited sulfur degassing. This observation aligns with findings from Apollo mare basalts, whose Zn isotope systematics also indicate limited degassing[29]. One plausible explanation is that thicker mare lava flows developed quenched surface crusts that suppressed volatile escape, thereby minimizing isotopic fractionation despite the Moon's low ambient pressure[29].

One troilite grain records a higher $\delta^{34}S$ value of 2.32 ± 0.47‰, which may reflect intragrain heterogeneity as CE-5 basalt and some lunar meteorites[28]. This could result from localized degassing through

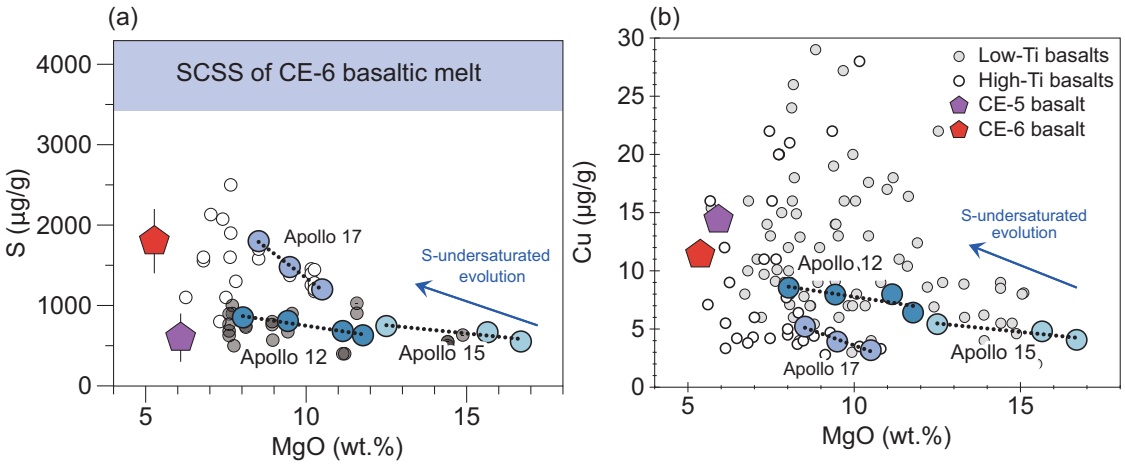

Fig. 3 | Sulfide-undersaturated evolution of lunar mare basalts. S (**a**) and Cu (**b**) contents in CE-6, CE-5, and Apollo mare basalts plotted against MgO. The sulfur contents at sulfide saturation (SCSS) of the CE-6 basaltic melt (**a**) was calculated using the silicate sulfur solubility model proposed by Ji and Dasgupta[27]. S and Cu contents in Apollo 12, 15, and 17 mare basalts[45] are highlighted, and the incompatible behavior of S (**a**) and Cu (**b**) in these magmas suggests sulfide-undersaturated evolution of most lunar mare basalts. Data source: The S content of CE-5 and Apollo samples are from the refs. 29,39. The Cu content of CE-6, CE-5 are from the literature[36,45,72] and Lunar Sample Compendium (https://wwwcurator.jsc.nasa.gov/lunar/lsc/index.cfm).

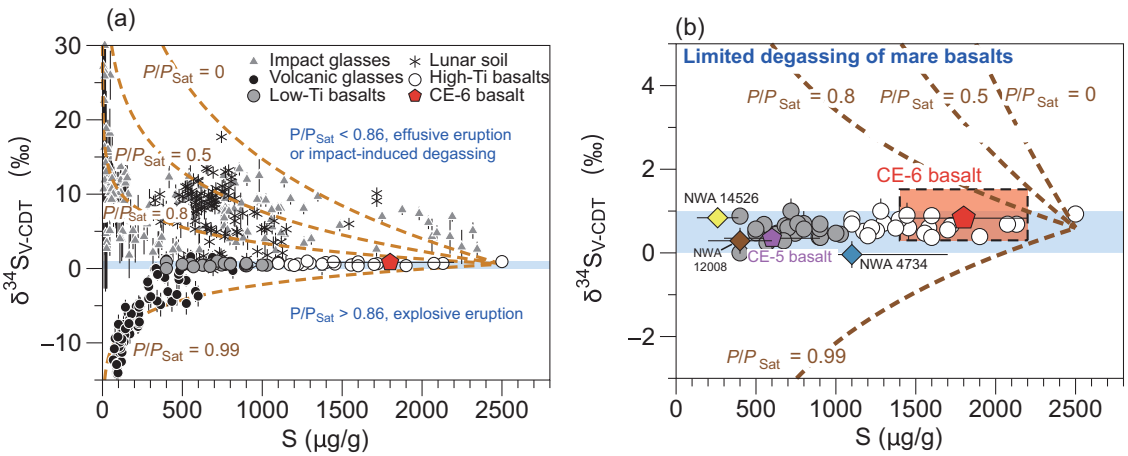

Fig. 4 | Sulfur isotope degassing under different eruption (effusive and explosive) and impact conditions. The modeled curves (brown dashed lines) with different P/P_{Sat} (effective vapor pressure relative to saturation pressure) are based on the lunar sulfur isotope degassing model from Gargano et al.[29] and Saal and Hauri[46] using an initial $\delta^{34}S$ value of 0.6‰ and an initial sulfur content of 2500 μg/g (**a**). In (**b**), the red shaded area denotes the $\delta^{34}S$ and sulfur content range observed in CE-6 basalts. The $\delta^{34}S$ values of CE-5 and Apollo mare basalts are from the literature[8,28,29] and references therein. Data for impact glasses and lunar soils are from the literature[32] and references therein, while volcanic glass data are sourced from the ref. 46.

open fractures or post-crystallization impact processing, as evidenced by the heavily fractured texture of the host clast (Fig. S5c). Such localized processes can generate isolated $\delta^{34}S$ enrichments without affecting the broader conclusion that CE-6 basalts experienced overall limited sulfur degassing.

Sulfur isotopic composition of the farside mantle and crust

Lunar basalts offer crucial insights into the Moon's mantle composition. The CE-6 low-Ti basalts, which erupted at ~2.8 Ga, originated from a highly depleted mantle region[32,33]. As there is no evidence for early sulfide saturation or significant magmatic degassing, their sulfur content (1800 ± 400 μg/g) and $\delta^{34}S$ value (0.83 ± 0.16‰) likely reflect the composition of the parental melt. Given the high SCSS (>2600 μg/g) of magma under lunar mantle conditions, the mantle source of CE-6 basalts—like other lunar mare basalts[25,27]—was likely sulfur-undersaturated during partial melting. Additionally, sulfur isotope fractionation between sulfide and silicate melt is minimal at high temperatures (~1300 °C; $\alpha_{melt-sulfide} \approx 0.999$)[43], suggesting that sulfur isotope fractionation during partial melting was negligible. Therefore, the $\delta^{34}S$ of the melt is considered a reliable proxy for the mantle source composition.

In addition to basalt clasts, the CE-6 landing site contains significant nonmare materials, primarily derived from the Chaffee S and other craters within the Apollo basin[47,48]. Our analyses revealed $\delta^{34}S$ values of 1.14 ± 0.60‰ and 0.94 ± 0.62‰ in troilite from noritic anorthosite and norite clasts, respectively. Petrographic observations suggest minimal alteration driven by impacts (Fig. 1b, c). Some sulfides exhibit elevated Ni contents, possibly attributable to the lower-temperature exsolution of Fe-Ni-Co sulfides and Fe-Ni-Cu sulfides[49,50] (Figs. S3c, S4). Consequently, these clasts likely preserve the sulfur isotopic composition of the farside crust of variable depth.

Mg-suite rocks are thought to form through partial melting of early magma-ocean cumulates at the base of the crust[51] during the Moon's early evolution[52]. Recent studies suggest that some Mg-suite-like (norite) clasts in the CE-6 soil crystallized at 4.25 Ga ago and likely represents a product of the South Pole–Aitken (SPA) impact melt sheet[35]. Notably, clasts with similar lithologic and geochemical characteristics have also been identified in Luna 20 samples from the

Crisium Basin, where they have been interpreted as Mg-suite rocks formed in the lower lunar crust[53]. Although the origin of the Mg-suite (or nortic) clasts in the CE-6 samples is beyond the scope of this study, the high Mg# (~77; Fig. S1) in pyroxene strongly suggests that they are generated from a deep, secondary crust. Taken together, basalt and Mg-suite clasts from the CE-6 landing site span a range of depths, source regions, and ages in the lunar farside mantle and crust. Despite these differences, their sulfur isotopic composition overlaps with each other (Fig. 2a), reinforcing the conclusion that the Moon's interior from the farside overall exhibits sulfur-isotope homogeneity, although they underwent diverse magmatic processes.

Large impact events on the Moon, such as those that formed the SPA and Apollo basins, are believed to have penetrated the lunar crust and excavated mantle materials[54–57]. Whether these impacts significantly modified the mantle's chemical composition remains uncertain. Since the CE-6 basalt erupted within the region of Apollo and SPA basins at ~2.8 Ga—later than both the SPA (~4.25–4.33 Ga)[35,58] and Apollo (~3.9–4.2 Ga) basins—it might have originated from a mantle region potentially influenced by these impacts. The nonmare clast either directly represents rocks crystallized from impact melt produced during the SPA-forming event[35], or may result from magmatic activity originating from the deep mantle[53], which may have escaped significant modification by the massive impact. The consistent $\delta^{34}S$ of the basalt, noritic anorthosite and norite clasts in the CE-6 samples implies that any impact-induced fractionation of sulfur isotopes during the SPA and Apollo impact events was minimal on the studied clasts in the present work. Nevertheless, only a limited number of crustal samples have been analyzed, and further investigations are required to fully assess the extent to which large impacts modified the Moon's farside mantle and crust compositions.

A global evaporation signature inherited from the giant impact

Existing lunar samples exhibit considerable variation in sulfur contents, with high-Ti basalts typically hosting higher sulfur levels than low-Ti basalts (Fig. 5a–c). The S/Dy ratios of mare basalts further demonstrate significant heterogeneity in the mantle sulfur budget (Fig. 5d), consistent with data from olivine-hosted melt inclusions (S/Dy: 50–200)[16–18]. Moreover, the lower S/Dy ratio compared with the MORB value (~212)[59] indicated that most Apollo basalts stem from a volatile-depleted lunar mantle source. Numerous studies have linked differences in radiogenic isotopes (e.g., variable Sr-Nd isotopes and μ values) among mare basalts and KREEP basalts to the incorporation of varying proportions of KREEP (or KREEP-like) components during mantle overturn[24]. The fact that mare basalts with distinct μ values and S/Dy ratio (Fig. 5d) suggest that sulfides were incorporated to different extents along with KREEP components, producing an uneven distribution of sulfur in the lunar mantle. This process likely happened during mantle overturn in the early stage of lunar evolution[19,20]. Nevertheless, given the relatively low sulfur content and high sulfide solubility for lunar magmas, the sulfides tend to have not crystallized until the very late stages of the LMO[26] and mare magmatism[24]. Thus, these mantle reservoirs maintain consistent sulfur isotopic compositions (Fig. 5e, f). KREEP-bearing cumulates (e.g., NWA 6950) also exhibit $\delta^{34}S$ values similar to those of other basalts, supporting the homogeneous $\delta^{34}S$ values among diverse basalt types and heterogenous lunar mantle.

Prior to the CE-6 mission, all sample-return landings were conducted in the nearside PKT, raising concerns that the observed isotopic signatures and volatile depletions may reflect local anomalies[23]. Uneven accretion during the giant impact[1] or large-scale impacts triggering urKREEP degassing[21,23] could produce such signatures. In this study, the CE-6 basalts returned from lunar farside display an elevated S/Dy ratio (184 ± 42) compared to many Apollo basalts (Fig. 5d), a result that may reflect either relative enrichment of S in the CE-6 mantle source or depletion in rare-earth elements[32,33]. Assuming a bulk silicate Earth (BSE) of Dy content (0.67 μg/g)[60] in the CE-6 mantle source, we estimate a sulfur concentration of 120 ± 30 μg/g, which is slightly higher but still within the upper range proposed for low-Ti basalt sources (79–120 μg/g)[17]. It further supports the idea of sulfur heterogeneity within the lunar mantle. Nevertheless, the $\delta^{34}S$ values of CE-6 basalts and nonmare clasts remain similar to those from nearside Apollo samples and meteorites (Figs. 2a and 6a), excluding a major contribution of localized phenomena or near- and farside asymmetry. It suggests that the lunar interior acquired a sulfur isotopic composition heavier than that of the BSE early in its history and has remained isotopically homogeneous through subsequent processes such as magmatic differentiation and eruption of mare basalts (Fig. 6b).

Because sulfur is both volatile and siderophile, its isotopic composition in the bulk silicate Moon (BSM) could be influenced by core-mantle differentiation, late accretion, and volatile evaporation. Experimental studies suggested that metal–silicate fractionation may favor lighter sulfur isotopes in the silicate phase[46,61]. This would result the LMO enriched in light sulfur isotopes, which is inconsistent with our result (Fig. S7a). In contrast, first-principles calculations by Wang et al.[62] proposed that such fractionation under lunar conditions would be minimal (<0.05‰) (Fig. S7b). Thus, the core formation hardly accounts for the ~2‰ heavier $\delta^{34}S$ observed on the BSM relative to the BSE.

Late accretion could also be a contributing factor. The low contents of highly siderophile elements in mare basalts suggest that late-accreted material added only ~0.02 wt.% of the Moon's mass into its mantle after core formation[63], with sulfur contributions estimated at <10%[45]. Among potential sources, only CM and CO chondrites show $\delta^{34}S$ values marginally overlapping with BSM[64] (Fig. S8). However, assuming a BSE-like initial $\delta^{34}S$ and a 10% chondritic input still fails to reproduce the observed Earth–Moon offset. More importantly, late accretion cannot explain the $\delta^{34}S$ of the Earth, which experienced a larger fraction of materials from the late accretion[62].

Therefore, the depletion of sulfur content and enrichment in heavy sulfur isotopes in the lunar interior relative to the BSE are best explained by the volatile evaporation process, consistent with patterns observed for other moderately volatile elements such as K and Zn[7,9]. Additionally, based on the sulfur isotopic composition of lunar impact glasses[32], we estimate isotopic fractionation factors ($\alpha_{gas-melt}$) in the range of ~0.995–0.998 for $\delta^{34}S$ during impact-induced events (Fig. S9a). Applying these fractionation factors, we estimate that 20–75% of lunar sulfur would have been lost to produce the observed $\delta^{34}S$ value of the BSM (Fig. S9b). Importantly, the globally homogeneous sulfur isotopic composition of the BSM rules out the possibility that the observed $\delta^{34}S$ signature reflects localized impact events[23]. Instead, it supports a global evaporation imprint inherited from the giant impact, either in the protolunar disk[7,9] or during tidally assisted magma ocean degassing[65,66]. This main conclusion is broadly consistent with a recent modeling work[67], which also highlights the role of the giant impact in driving volatile loss and sulfur isotope fractionation.

Despite the homogeneity in sulfur isotopic composition across the lunar interior, the variation of sulfur contents and Dy/S ratios of different mantle domains[16,17] suggests that complex post-formation processes, such as mantle overturn, have significantly modified the distribution of sulfur, Nd–Pb isotopic signatures, and possibly other volatile elements within the lunar mantle. Future analyses of the isotopic composition of other volatile elements (e.g., Cl, K, Rb, Cu and Zn) in lunar farside samples will be essential for further testing this model.

Methods

CE-6 samples and petrological analyses

The scooped CE-6 soil (CE6C0200YJFM003, 500 mg) was obtained from the China National Space Administration Agency. Hundreds of lithic fragments with the size exceeding 50 μm were manually picked out from the CE-6 soil. Then, they were subsequently mounted in resin

https://doi.org/10.1038/s41467-025-60743-z

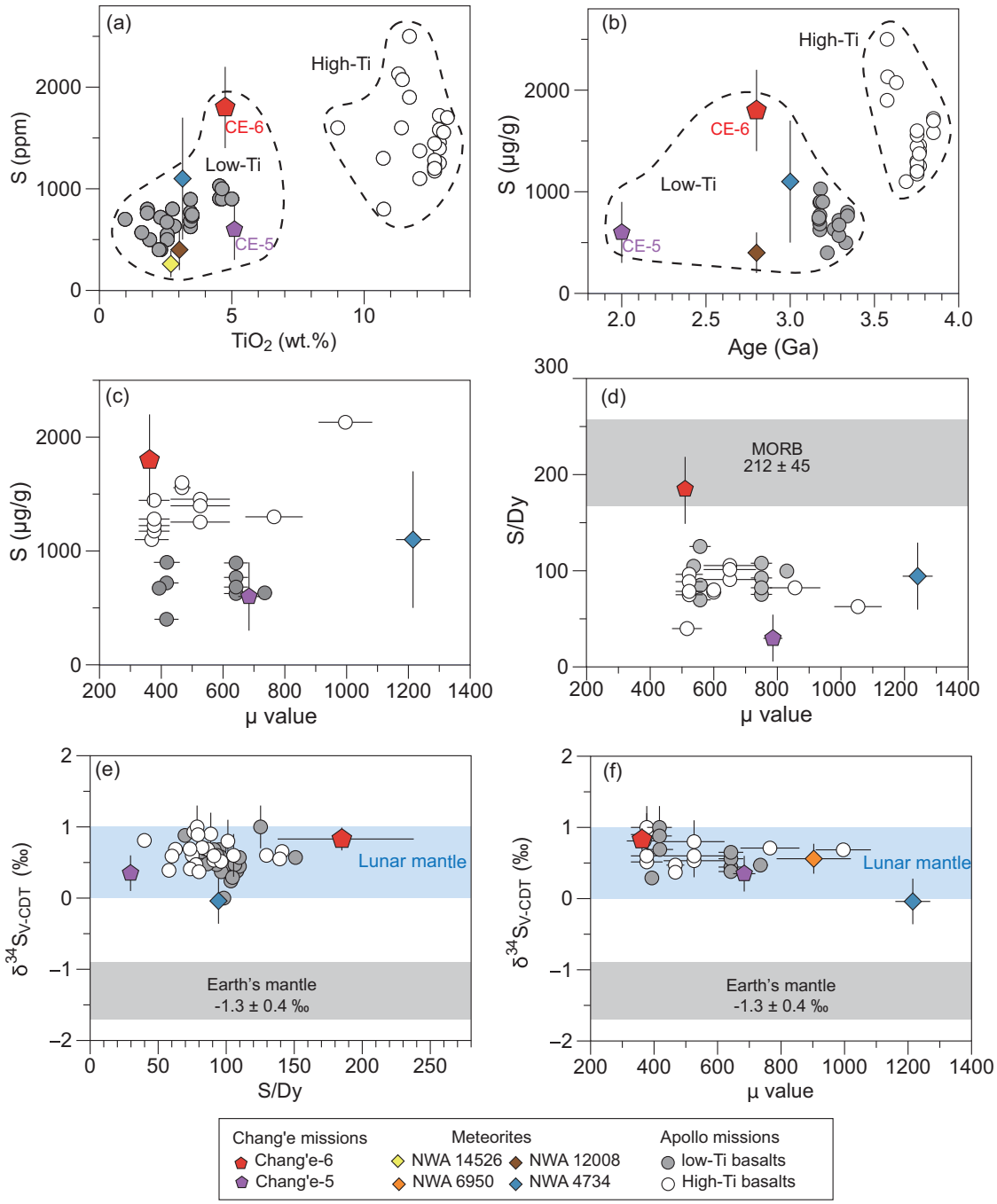

Fig. 5 | Comparison of lunar farside and nearside basalts and other basaltic meteorites. Mare basalts show variable S content with high-Ti basalt higher than low-Ti basalts (**a**–**c**). The S/Dy of both low-Ti and high-Ti basalts are variable and lower than that of mid-ocean ridge basalts (212 ± 45)[59] (**d**). The $\delta^{34}S$ values further show a global homogeneity (0–1‰), although mantle domains are very heterogenous (**e**, **f**). Data source: The $\delta^{34}S$ values of meteorites (NWA 4734 and NWA 6950) are from the ref. 28. Ages of CE-6, CE-5, meteorites and Apollo basalts are from the refs. 24,32,33,73. The μ values ($^{238}U/^{204}Pb$ ratio) of CE-6, CE-5, meteorites and Apollo basalts are from the literature[33] and references therein.

sections for detailed petrological and geochemical analyses (Fig. 1). These clasts include basalt clasts, breccias and nonmare clasts (e.g., Mg-suite clasts). Two lunar low-Ti basaltic meteorites (NWA 14526 and NWA 12008) are also analyzed for comparison.

The lithic fragments were analyzed by TESCAN Integrated Mineral Analyzer system (TIMA3 X GHM) at China University of Geosciences, Wuhan. Detailed methods for TIMA analyses can be found in Wang et al.[28]. The combination of TIMA measurements with BSE images and X-ray spectra can identify individual grains and locate grain boundaries. The number of pixels of each grain phase was then converted into the relative surface area as a modal percentage. Based on this, the system automatically compared the measured BSE and EDS data of each phase with a built-in classification scheme, distinguished mineral phases of basaltic clasts, and then computed mineral volumetric fractions (Fig. S2).

Major elements of minerals

Major elemental compositions of different minerals were determined using a JEOL JXA-8230 electron microprobe analyzer at the State Key Laboratory of Geological Processes and Mineral Resources, China

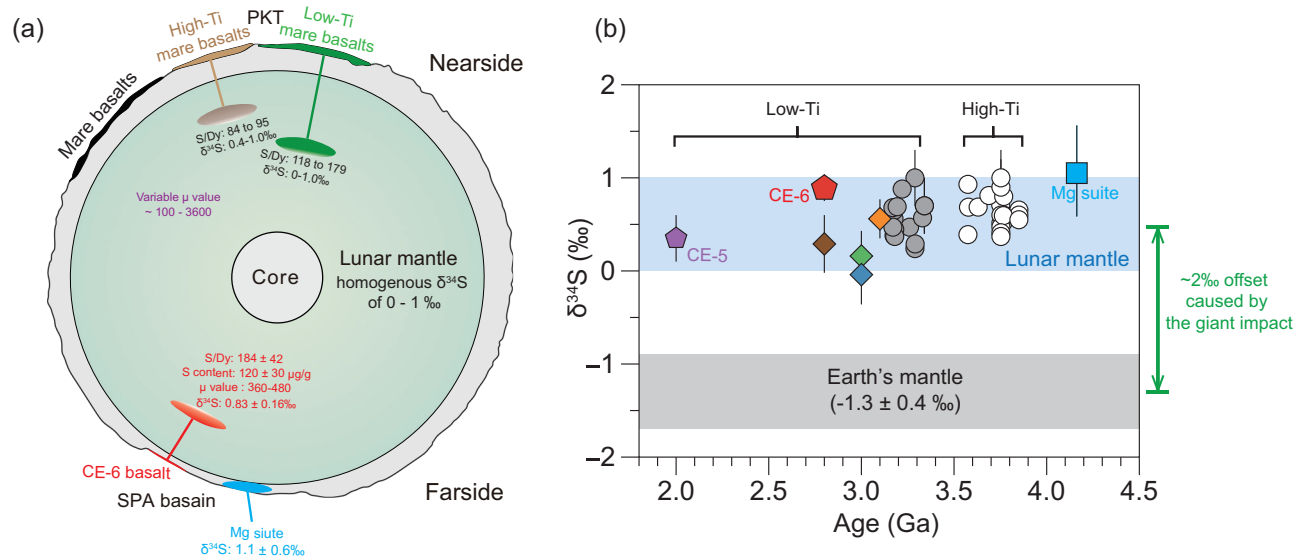

Fig. 6 | Distribution of S/Dy, μ value and $\delta^{34}S$ in the lunar mantle of different regions. The lunar mantle demonstrates significant variation on S contents and μ values (**a**), but their sulfur isotopes remain consistent after volatile loss induced by the giant impact, regardless of ages of basalts and Mg-suite rocks (**b**). Symbols follow the same legend as in Fig. 5; the green diamond represents NWA 10597.

University of Geosciences, Wuhan (GPMR-CUG). The focused beam was typically at 3 μm diameter for silicate and 1 μm (spot analysis mode) for sulfides. For silicate phases, the standards used for ZAF matrix correction were jadeite (Na), olivine (Si), diopside (Ca, Mg), almandine (Fe, Al), sanidine (K), rutile (Ti), rhodonite (Mn), and chromium oxide (Cr). For sulfides, the standards were hematite (Fe), pyrite (S), pentlandite (Ni), cobalt (Co), chalcopyrite (Cu) and chromite (Cr), with an alloy standard for Fe–Ni metals. Some grains were mapped for expected major and minor elements (e.g., S, Fe, Ni, Co, and Cu) (Fig. S3).

Laser ablation MC-ICP-MS for sulfur isotopes

In this study, we performed in-situ sulfur isotopes analysis in troilites with an ESI NWR FemtoUC femtosecond laser ablation system (New Wave Research, Fremont, CA, USA) coupled to a Neptune Plus MC-ICP-MS instrument (Thermo Fisher Scientific, Germany) at the GPMR. Given ultrafast energy deposition, the femtosecond laser ablation system can significantly reduce the matrix effect and is a convenient and robust approach for in-situ sulfur isotopic analyses of extraterrestrial samples which have achieved similar analytical uncertainty with Nano SIMS[28]. A frequency of 10 Hz with 5 s^{-1} ablation for a total of 80 pulses was used, allowing high spatial-resolution analyses of 8-μm spot sizes in this study[28,68]. Detailed analytical strategies and data quality of this method has also been discussed in Wang et al.[28].

The pyrite reference PPP-1[69] with $\delta^{34}S_{V\text{-}CDT} = 5.3 \pm 0.2‰$ was used as an external standard. The pyrrhotite reference YP136 and troilites from two iron meteorites (Muonionalusta and NWA 859) were analyzed as unknown samples to monitor data quality. The YP136 show $\delta^{34}S_{V\text{-}CDT} = 1.46 \pm 0.48‰$ ($n = 10$, 2 SD) within the range of reference values ($1.5 \pm 0.3‰$)[70] (Table S5 and Fig. S10). The $\delta^{34}S_{V\text{-}CDT}$ of troilites in Muonionalusta and NWA 859 are $0.12 \pm 0.48‰$ and $0.45 \pm 0.50‰$, respectively, overlapping with the values reported before[28]. The results are also consistent with the $\delta^{34}S_{V\text{-}CDT}$ of iron meteorites measured using a ThermoFinnigan MAT 253 mass spectrometer[71]. The reproducibility of the reference materials suggests that the external uncertainty in this study is 0.50‰ (2sd) for $\delta^{34}S_{V\text{-}CDT}$, which is comparable to sulfur isotopes obtained by nano-SIMS[39].

Data availability

All data generated and analyzed during this study are included in the Supplementary Information files. The sulfur isotope and mineralogical data generated in this study have been deposited in the Figshare database under accession code https://doi.org/10.6084/m9.figshare.29136590.

References

1. Canup, R. M., Visscher, C., Salmon, J. & Fegley, B. Jr. Lunar volatile depletion due to incomplete accretion within an impact-generated disk. *Nat. Geosci.* **8**, 918–921 (2015).
2. Young, E. D. et al. Oxygen isotopic evidence for vigorous mixing during the Moon-forming giant impact. *Science* **351**, 493–496 (2016).
3. Schiller, M., Bizzarro, M. & Fernandes, V. A. Isotopic evolution of the protoplanetary disk and the building blocks of Earth and the Moon. *Nature* **555**, 507–510 (2018).
4. Zhang, J., Dauphas, N., Davis, A. M., Leya, I. & Fedkin, A. The proto-Earth as a significant source of lunar material. *Nat. Geosci.* **5**, 251–255 (2012).
5. Mougel, B., Moynier, F. & Göpel, C. Chromium isotopic homogeneity between the Moon, the Earth, and enstatite chondrites. *Earth Planet. Sci. Lett.* **481**, 1–8 (2018).
6. Sharp, Z. D., Shearer, C. K., McKeegan, K. D., Barnes, J. D. & Wang, Y. Q. The chlorine isotope composition of the Moon and implications for an anhydrous mantle. *Science* **329**, 1050–1053 (2010).
7. Paniello, R. C., Day, J. M. D. & Moynier, F. Zinc isotopic evidence for the origin of the Moon. *Nature* **490**, 376–379 (2012).
8. Wing, B. & Farquhar, J. Sulfur isotope homogeneity of lunar mare basalts. *Geochim. Cosmochim. Acta* **170**, 266–280 (2015).
9. Wang, K. & Jacobsen, S. B. Potassium isotopic evidence for a high-energy giant impact origin of the Moon. *Nature* **538**, 487–490 (2016).
10. Pringle, E. A. & Moynier, F. Rubidium isotopic composition of the Earth, meteorites, and the Moon: Evidence for the origin of volatile loss during planetary accretion. *Earth Planet. Sci. Lett.* **473**, 62–70 (2017).
11. Haskin, L. & Warren, P. Lunar Chemistry. In *Lunar Sourcebook* 357–474 (Cambridge University Press, 1991).
12. Day, J. M. D. & Moynier, F. Evaporative fractionation of volatile stable isotopes and their bearing on the origin of the Moon. *Philos. Trans. R. Soc. A.* **372**, 20130259 (2014).

13. Saal, A. E. et al. Volatile content of lunar volcanic glasses and the presence of water in the Moon's interior. *Nature* **454**, 192–195 (2008).
14. Robinson, K. L. & Taylor, G. J. Heterogeneous distribution of water in the Moon. *Nat. Geosci.* **7**, 401–408 (2014).
15. McCubbin, F. M. et al. Magmatic volatiles (H, C, N, F, S, Cl) in the lunar mantle, crust, and regolith: abundances, distributions, processes, and reservoirs. *Am. Min.* **100**, 1668–1707 (2015).
16. Su, X. & Zhang, Y. Volatiles in melt inclusions from lunar mare basalts: bridging the gap in the H2O/Ce ratio between melt Inclusions in lunar pyroclastic sample 74220 and other mare samples. *Geochim. Cosmochim. Acta* **373**, 232–244 (2024).
17. Ni, P., Zhang, Y., Chen, S. & Gagnon, J. A melt inclusion study on volatile abundances in the lunar mantle. *Geochim. Cosmochim. Acta* **249**, 17–41 (2019).
18. Chen, Y. et al. Water, fluorine, and sulfur concentrations in the lunar mantle. *Earth Planet. Sci. Lett.* **427**, 37–46 (2015).
19. Elkins Tanton, L. T., Van Orman, J. A., Hager, B. H. & Grove, T. L. Re-examination of the lunar magma ocean cumulate overturn hypothesis: melting or mixing is required. *Earth Planet. Sci. Lett.* **196**, 239–249 (2002).
20. Shearer, C. K. Thermal and magmatic evolution of the Moon. *Rev. Mineral. Geochem.* **60**, 365–518 (2006).
21. Barnes, J. J. et al. Early degassing of lunar urKREEP by crust-breaching impact(s). *Earth Planet. Sci. Lett.* **447**, 84–94 (2016).
22. Jolliff, B. L., Gillis, J. J., Haskin, L. A., Korotev, R. L. & Wieczorek, M. A. Major lunar crustal terranes: surface expressions and crust-mantle origins. *J. Geophys. Res.: Planets* **105**, 4197–4216 (2000).
23. Tartèse, R., Sossi, P. & Moynier, F. Conditions and extent of volatile loss from the Moon during formation of the Procellarum basin. *Proc. Natl. Acad. Sci USA* **118**, e2023023118 (2021).
24. Merle, R. E. et al. Pb-Pb ages and initial Pb isotopic composition of lunar meteorites: NWA 773 clan, NWA 4734, and Dhofar 287. *Meteorit. Planet. Sci.* **55**, maps.13547 (2020).
25. Ding, S., Hough, T. & Dasgupta, R. New high pressure experiments on sulfide saturation of high-FeO∗ basalts with variable TiO2 contents—implications for the sulfur inventory of the lunar interior. *Geochim. Cosmochim. Acta* **222**, 319–339 (2018).
26. Steenstra, E. S. et al. The fate of sulfur and chalcophile elements during crystallization of the lunar magma ocean. *J. Geophys. Res. Planets* **125**, e2019JE006328 (2020).
27. Ji, D. & Dasgupta, R. Sulfur inventory of the young lunar mantle constrained by experimental sulfide saturation of Chang'e-5 mare basalts and a new sulfur solubility model for silicate melts in equilibrium with sulfides of variable metal–sulfur ratio. *Geochim. Cosmochim. Acta* **394**, 284–297 (2025).
28. Wang, Z. et al. Sulfide compositions of young Chang'e-5 basalts and implications for sulfur isotopes in lunar basalt sources. *Geochim. Cosmochim. Acta* **368**, 168–184 (2024).
29. Gargano, A. et al. The Zn, S, and Cl isotope compositions of mare basalts: implications for the effects of eruption style and pressure on volatile element stable isotope fractionation on the Moon. *Am. Min.* **107**, 1985–1994 (2022).
30. Labidi, J., Cartigny, P. & Moreira, M. Non-chondritic sulphur isotope composition of the terrestrial mantle. *Nature* **501**, 208–211 (2013).
31. Li, C. et al. Nature of the lunar far-side samples returned by the Chang'E-6 mission. *Natl. Sci. Rev.* **11**, nwae328 (2024).
32. Cui, Z. et al. A sample of the Moon's far side retrieved by Chang'e-6 contains 2.83-billion-year-old basalt. *Science* **0**, eadt1093 (2024).
33. Zhang, Q. W. L. et al. Lunar farside volcanism 2.8 billion years ago from Chang'e-6 basalts. *Nature* 1–2. https://doi.org/10.1038/s41586-024-08382-0 (2024).
34. Che, X. et al. Isotopic and compositional constraints on the source of basalt collected from the lunar farside. *Science* **387**, 1306–1310 (2025).
35. Su, B. *et al*. South Pole–Aitken massive impact 4.25 billion years ago revealed by Chang'e-6 samples. *Natl. Sci. Rev*. nwaf103. https://doi.org/10.1093/nsr/nwaf103 (2025).
36. Wang, Z. et al. Chemical compositions of Chang'e-6 lunar soil and substantial addition of noritic crust ejecta from Apollo basin. *Geology* https://doi.org/10.1130/G53086.1 (2025).
37. Elardo, S. et al. The origin of young mare basalts inferred from lunar meteorites Northwest Africa 4734, 032, and LaPaz Icefield 02205. *Meteorit. Planet. Sci.* **49**, 261–291 (2014).
38. Steenstra, E. S. & van Westrenen, W. Sulfides in the Moon. In *Encyclopedia of Lunar Science* (ed. Cudnik, B.) 1–6, https://doi.org/10.1007/978-3-319-05546-6_119-1 (Springer International Publishing, 2017).
39. Liu, X. et al. Sulfur isotopic fractionation of the youngest Chang'e-5 basalts: constraints on the magma degassing and geochemical features of the mantle source. *Geophys. Res. Lett.* **49**, e2022GL099922 (2022).
40. Kerridge, J. F., Kaplan, I. R., Petrowski, C. & Chang, S. Light element geochemistry of the Apollo 16 site. *Geochim. Cosmochim. Acta* **39**, 137–162 (1975).
41. Moynier, F., Albarède, F. & Herzog, G. F. Isotopic composition of zinc, copper, and iron in lunar samples. *Geochim. Cosmochim. Acta* **70**, 6103–6117 (2006).
42. Dottin, J. W. III et al. Isotopic evidence of sulfur photochemistry during lunar regolith formation. *Geochem. Perspect. Lett.* **23**, 38–42 (2022).
43. Marini, L., Moretti, R. & Accornero, M. Sulfur isotopes in magmatic-hydrothermal systems, melts, and magmas. In *Sulfur in Magmas and Melts: Its Importance for Natural and Technical Processes* Vol. 73 (eds Behrens, H. & Webster, J. D.) 423–492 (Mineralogical Soc Amer & Geochemical Soc, 2011).
44. Brenan, J. M., Mungall, J. E. & Bennett, N. R. Abundance of highly siderophile elements in lunar basalts controlled by iron sulfide melt. *Nat. Geosci.* **12**, 701–706 (2019).
45. Gleißner, P., Salme, J. & Becker, H. Siderophile volatile element inventory in lunar magmatic rocks and mantle sources. *Earth Planet. Sci. Lett.* **593**, 117680 (2022).
46. Saal, A. & Hauri, E. Large sulfur isotope fractionation in lunar volcanic glasses reveals the magmatic differentiation and degassing of the Moon. *Sci. Adv.* **7**, eabe4641 (2021).
47. Xu, L., et al. Chronology, local stratigraphy, and foreign ejecta materials at the chang'e-6 landing site: constraints on the provenance of samples returned from the Moon's farside. *Geophys. Res. Lett.* **51**, e2024GL111311 (2024).
48. Gou, S. et al. Complex basalt evolution in the Chang'e-6 landing area. *Earth Planet. Sci. Lett.* **648**, 119091 (2024).
49. Etschmann, B., Pring, A., Putnis, A., Grguric, B. A. & Studer, A. A kinetic study of the exsolution of pentlandite (Ni, Fe)$_9$ S$_8$ from the monosulfide solid solution (Fe, Ni)S. *Am. Min.* **89**, 39–50 (2004).
50. Vaughan, D. J. Chemical bonding in sulfide minerals. *Rev. Mineral. Geochem.* **61**, 231–264 (2006).
51. Shearer, C. K., Elardo, S. M., Petro, N. E., Borg, L. E. & McCubbin, F. M. Origin of the lunar highlands Mg-suite: an integrated petrology, geochemistry, chronology, and remote sensing perspective. *Am. Min.* **100**, 294–325 (2015).
52. Borg, L. E. & Carlson, R. W. The evolving chronology of Moon formation. *Annu. Rev. Earth Planet. Sci.* **51**, 25–52 (2023).
53. Shearer, C. K., Moriarty, D. P., Simon, S. B., Petro, N. & Papike, J. J. Where is the lunar mantle and deep crust at crisium? A perspective from the luna 20 samples. *J. Geophys. Res.: Planets* **128**, e2022JE007409 (2023).
54. Potter, R. W. K., Collins, G. S., Kiefer, W. S., McGovern, P. J. & Kring, D. A. Constraining the size of the South Pole-Aitken basin impact. *Icarus* **220**, 730–743 (2012).

55. Potter, R. W. K., Head, J. W., Guo, D., Liu, J. & Xiao, L. The Apollo peak-ring impact basin: insights into the structure and evolution of the South Pole–Aitken basin. *Icarus* **306**, 139–149 (2018).
56. Melosh, H. J. et al. South Pole–Aitken basin ejecta reveal the Moon's upper mantle. *Geology* **45**, 1063–1066 (2017).
57. Citron, R. I., Smith, D. E., Stewart, S. T., Hood, L. L. & Zuber, M. T. The South Pole-Aitken basin: constraints on impact excavation, melt, and ejecta. *Geophys. Res. Lett.* **51**, e2024GL110034 (2024).
58. Joy, K. H. et al. Evidence of a 4.33 billion year age for the Moon's South Pole–Aitken basin. *Nat. Astron*. https://doi.org/10.1038/s41550-024-02380-y (2024).
59. Kovalenko, V. I., Naumov, V. B., Girnis, A. V., Dorofeeva, V. A. & Yarmolyuk, V. V. Estimation of the average contents of H2O, Cl, F, and S in the depleted mantle on the basis of the compositions of melt inclusions and quenched glasses of mid-ocean ridge basalts. *Geochem. Int.* **44**, 209–231 (2006).
60. Mcdonough, W. & Sun, S. The composition of the EARTH. *Chem. Geol.* **120**, 223–253 (1995).
61. Labidi, J. et al. Experimentally determined sulfur isotope fractionation between metal and silicate and implications for planetary differentiation. *Geochim. Cosmochim. Acta* **175**, 181–194 (2016).
62. Wang, W. et al. Sulfur isotopic signature of Earth established by planetesimal volatile evaporation. *Nat. Geosci*. https://doi.org/10.1038/s41561-021-00838-6 (2021).
63. Day, J. M. D. & Walker, R. J. Highly siderophile element depletion in the Moon. *Earth Planet. Sci. Lett.* **423**, 114–124 (2015).
64. Alexander, C. M. O., Wynn, J. G. & Bowden, R. Sulfur abundances and isotopic compositions in bulk carbonaceous chondrites and insoluble organic material: clues to elemental and isotopic fractionations of volatile chalcophiles. *Meteor. Planet. Sci.* **57**, 334–351 (2022).
65. Charnoz, S. et al. Tidal pull of the Earth strips the proto-Moon of its volatiles. *Icarus* **364**, 114451 (2021).
66. Madeira, G., Esteves, L., Charnoz, S., Lega, E. & Moynier, F. Hydrodynamical simulations of proto-Moon degassing. *Earth Planet. Sci. Lett.* **651**, 119163 (2025).
67. Fu, H. & III, J. Post-giant-impact lunar sulfur and sulfur isotope coevolution: insights into the Moon's origin. In *56th Lunar and Planetary Science Conference Abstract #1616* (Lunar and Planetary Institute, Houston, 2025).
68. Feng, Y. et al. A new analytical mode and application of the laser ablation inductively coupled plasma mass spectrometer in the earth sciences. *Sci. China Earth Sci.* **65**, 182–196 (2022).
69. Gilbert, S. E. et al. Optimisation of laser parameters for the analysis of sulphur isotopes in sulphide minerals by laser ablation ICP-MS. *J. Anal. Spectrom.* **29**, 1042–1051 (2014).
70. Li, R., Xia, X., Yang, S., Chen, H. & Yang, Q. Off-mount calibration and one new potential pyrrhotite reference material for sulfur isotope measurement by secondary ion mass spectrometry. *Geostand. Geoanalytical Res.* **43**, 177–187 (2019).
71. Antonelli, M. A. et al. Early inner solar system origin for anomalous sulfur isotopes in differentiated protoplanets. *Proc. Natl. Acad. Sci. USA* **111**, 17749–17754 (2014).
72. Wang, Z. et al. Young KREEP-like mare volcanism from Oceanus Procellarum. *Geochim. Cosmochim. Acta* **373**, 17–34 (2024).
73. Snape, J. F. et al. The timing of basaltic volcanism at the Apollo landing sites. *Geochim. Cosmochim. Acta* **266**, 29–53 (2019).

Acknowledgements

We thank the China National Space Administration for providing the Chang'e-6 samples.This work was supported by Scientific Research Innovation Capability Support Project for Young Faculty (ZYGXQNJSKYCXNLZCXM-P6), the National Natural Science Foundation of China (No. 42441802 and No. 42241156) and Hubei Provincial Natural Science Foundation of China (No. 2025AFA005). Y.H.L. thanks the support of CSC scholarship (No. 202406410015).

Author contributions

Z.C.W. and Y.H.L. designed the research and applied for the CE-6 samples. F.M. and J.S. helped in refining the ideas. Y.H.L., Z.C.W., W.Z., Z.C.H., J.Q.Z., and X.C. measured the sulfur isotopes of troilites, Y.H.L., Z.C.W., K.Q.Z., Z.B.S., Q.H., J.Q.Z., T.Y.L., F.B.P., X.C., L.X., X.W., and K.C. prepared samples and obtained EMPA and TIMA data. Y.S.L. and Z.C.H. provided access to the experimental platforms. Y.H.L. and Z.C.W. wrote the manuscript draft, and all other authors participated in the data interpretation and editing of the manuscript.

Competing interests

The authors declare no competing interests.

Additional information

Supplementary information The online version contains supplementary material available at https://doi.org/10.1038/s41467-025-60743-z.

Correspondence and requests for materials should be addressed to Zaicong Wang.

Peer review information *Nature Communications* thanks the anonymous reviewers for their contribution to the peer review of this work. A peer review file is available.